A new modeling of the dissolution of chromia in Na2O-SiO2 liquids

V. Szczepan, F. Brix, C. Petitjean, P.J. Panteix, M. Vilasi

A new modeling of the dissolution of chromia in Na_2O-SiO_2 liquids

V. Szczepan[1], F. Brix[1], C. Petitjean[1], P.J. Panteix[1], M. Vilasi[1]

[1]Université de Lorraine, CNRS, IJL, F-54011 Nancy, France

Abstract

A model of dissolution of chromia in binary Na_2O-SiO_2 liquids is presented in this work. Data available in the literature on the acid/base properties and the chemistry of chromium in such liquids were used in order to refine the model. Physical phenomena such as migration of ions and the resulting electric field, the mechanical equilibrium of the liquid and the interface recession caused by the dissolution of chromia are also implemented in the model. Numerical simulation has been compared to experimental measurements of Na_2O, SiO_2 and Cr_2O_3 concentration profiles after 1 hour of immersion of chromia in a $(Na_2O)_{0.25}(SiO_2)_{0.75}$ liquid at 1150 °C. The phenomena having a significant influence on the dissolution rate of chromia are highlighted in the last part of this paper.

Keywords

glass, chromia, dissolution, thermochemistry, modeling, numerical simulation.

List of symbols

Q^n	silica tetrahedron holding n bridging oxygens
a_i	activity of the chemical species i
K_n	equilibrium constant between Q^n, Q^{n-1} and Na_2O.
λ	molar fraction of Na_2O in binary $(Na_2O)_\lambda(SiO_2)_{1-\lambda}$
X	oxygen valence of Cr^{III}
Y	oxygen valence of Cr^{VI}
Z	oxygen valence of Cr^{II}
K_d	equilibrium constant of dissolution of Cr_2O_3
K_o	equilibrium constant of oxidation of Cr^{III} in molten silicates
K_r	equilibrium constant of reduction of Cr^{III} in molten silicates
P_{O_2}	external oxygen pressure (atm)
x_{Cr}	atomic fraction of chromium in the liquid
H_{O_2}	Henry constant of O_2 ($mol.m^{-3}.atm^{-1}$)
C_i	concentration of the chemical species i ($mol.m^{-3}$)
C_{total}	total atomic concentration in the liquid ($mol.m^{-3}$)
K_j'	equilibrium constant of the simplified reaction j expressed as a function of concentrations
ξ_j	reaction rate ($mol.m^{-3}.s^{-1}$)
kc_j	kinetic constant of the reaction j
$v_{i,j}$	stoichiometric coefficient of the compound i in the reaction j
$\vec{J_i}$	flux of the chemical species i ($mol.m^{-2}.s^{-1}$)
D_i	diffusion coefficient of the chemical species i ($m^2.s^{-1}$)
R	ideal gas constant ($J.mol^{-1}.K^{-1}$)
T	temperature (K)
$\tilde{\mu}_i$	electro-chemical potential of the species i ($J.mol^{-1}$)

$\vec{V}$	velocity field in the liquid ($m.s^{-1}$)
z_i	electric charge of the chemical species i ($C.mol^{-1}$)
$\vec{E}$	electric field in the liquid ($V.m^{-1}$)
$\hat{v}$	normalized volume
V_{m_i}	molar volume of the species i
$\tau_{\hat{v}}$	production rate of the normalized volume (s^{-1})
χ	molar fraction of Na_2O in the ternary $(Na_2O)_\chi(SiO_2)_\gamma(O_2)_\zeta$
γ	molar fraction of SiO_2 in the ternary $(Na_2O)_\chi(SiO_2)_\gamma(O_2)_\zeta$
ζ	molar fraction of O_2 in the ternary $(Na_2O)_\chi(SiO_2)_\gamma(O_2)_\zeta$
e	chromia layer thickness (m)
S_{Cr}	solubility of chromium in the liquid ($mol.m^{-3}$)
D_{Cr}^{App}	diffusion coefficient of total chromium in the liquid ($m^2.s^{-1}$)
k_d	parabolic dissolution constant of chromia ($m^2.s^{-1}$)
P	Cr^{III}/Cr ratio in the liquid
C_{Cr}^{App}	total Cr concentration in the liquid
x	distance from the liquid/oxide interface in the liquid (m)
t	time (s)

1. Introduction

The contact between an alloy and a silica-based liquid at high temperature is a commonly encountered issue in glass industries such as nuclear waste vitrification [1] or glass fiber production [2,3]. Nickel-based or cobalt-based super-alloys containing a large amount of chromium offer an interesting solution for these applications. They show a good balance between hardness and ductility in comparison to ceramics or noble metals (i.e. platinum). Moreover, they have a high corrosion resistance at high temperature due to the formation of a protective chromia (Cr_2O_3) layer with low solubility in molten glass [4]. In the case of commercial and waste vitrification glasses, which do not contain iron oxide (or any oxide able to form a spinel with chromia), the chromium oxide layer is in direct contact with the liquid and thus, prevents the fast active corrosion of the alloy. The dissolution rate of chromia is the key to predict the lifetime of alloys in industrial processes.

The dissolution of chromia in silica-based liquids is a complex problem of diffusion coupled with chemical reactions. Consequently, the prediction of the dissolution rate of the chromia or the identification of the parameters influencing the dissolution rate is thus difficult. A model of the dissolution of chromia in molten glasses might be a useful tool. Since the parameters such as diffusion coefficient or chemical equilibrium are known, the prediction of the dissolution rate of the oxide is possible. Recently, Schmucker *et al.* [5] have postulated that the dissolution of chromia is limited by the diffusion of chromium in the liquid. The parameters of the dissolution such as the diffusion coefficient of chromium in the liquid can be determined by various methods, such as square wave voltammetry [6–9], molecular dynamics calculation [10,11] or Electron Probe Micro Analysis (EPMA) [12]. Various chemical reactions of chromium in molten silicate have also been identified [13,14] with the associated thermodynamic data.

In this paper, a model of the dissolution of chromia in simple Na_2O-SiO_2 liquids is proposed. Various physical phenomena such as electro-neutrality of the liquid, interface recession and mechanical equilibrium are considered in addition to the chemical diffusion and equilibria. Simple procedures are proposed in order to implement these phenomena in a mathematical model that can be easily solved. The thermodynamic data have been determined from data available in the literature. The Ni-30(wt%.)Cr alloy has been oxidized in order to form a thick chromia layer. The alloy has then been immersed in a simple $(Na_2O)_{0.25}(SiO_2)_{0.75}$ liquid at 1150 °C and the diffusion profile of chromium has been measured by EPMA at room temperature. The obtained results were compared to the simulation. Eventually, the phenomena having a significant influence on the dissolution rate of chromia are identified showing that a simplification of the model is possible when considering certain assumptions. This simplification can become the basis of a model that could be used to study the corrosion of chromia forming alloys in molten glasses and thus optimize their lifetime in industrial processes.

2. Materials and methods

2.1. Glass and alloy elaboration

The selected Ni-30Cr alloy was elaborated by high frequency induction melting in argon atmosphere, in order to avoid the oxidation of chromium. Ingot of 3 kg was melted from pure chromium (Alfa Aesar chromium pieces, 3 – 8 mm (0.1 - 0.31 in), 99.99%) and pure nickel (Alfa Aesar nickel shot, 3 – 25 mm (0.1 - 0.98 in), 99.95%); more details about the synthesis and the characterization of the alloy can be found in reference [15]. Rods were cut from the ingot with dimensions 25 mm × 5 mm × 3 mm, polished to P1200 and ultrasonically cleaned in ethanol.

The $(Na_2O)_{0.25}(SiO_2)_{0.75}$ glass (N3S) was elaborated by the Cerfav (Centre Européen de Recherche et de Formation aux Arts Verriers) from SiO_2 and Na_2CO_3 powders. The composition of the obtained glass was analyzed by EPMA, the results are available in reference [5].

2.2. Immersion tests

The Ni-30Cr rod was sealed into a "T" shape alumina device which maintains the sample immersed in the glass contained in a $Pt_{95}Au_5$ (FKS) crucible (inner diameter: 30 mm, height: 30 mm). The crucible contains 15 g of glass which corresponds to 20 mm depth for immersing the sample while avoiding the contact between the alloy and the crucible and the contact between the glass and the alumina.

The sample was first oxidized in air at 1150 °C during 24 hours in order to develop a thick chromia layer (around 10 µm) on the surface of the sample [15,16]. The glass was melted and maintained at 1150 °C during 1 hour before the immersion to ensure the thermal and the chemical equilibrium of the liquid. The sample is then immersed for 1 hour. This duration is optimized to obtain a diffusion profile of chromium over several hundreds of µm while avoiding the chromium to reach the convective zone far from the interface. The sample (alloy + glass) is then quenched, removed and embedded in resin before being cut for cross-section characterizations. The section is polished with SiC grinding paper (P1200 to P4000) and diamond gel (1 µm). Immersion tests were also performed with sintered pure chromia rods but samples ended up systematically destroyed after quenching due to stresses between the chromia and the glass. The best results were obtained with the chromia-forming alloy.

2.3. EPMA characterization

The EPMA characterizations were performed with a JXA 8530F (JEOL) equipped with 5 Wavelength Dispersive X-ray Spectroscopy (WDS) analyzers. The electron beam was defocused to probe an area of 20 µm of diameter in order to integrate all the Na^+ ions prone to

migrate out of the analyzed glass volume due to their interaction with the electron beam. Albite ($NaAlSi_2O_8$) was used as standard for silicon and sodium and chromia was used for chromium. Oxygen was quantified using the stoichiometry of the oxide SiO_2 (for Si), Na_2O (for Na) and Cr_2O_3 (for Cr). The analysis current was 10 nA and the analysis time was 10 seconds. The obtained result is the composition of the glass in mass fraction of SiO_2, Na_2O and Cr_2O_3.

3. Thermochemistry of the Na_2O-SiO_2-O_2-Cr_2O_3 system

3.1. Acid/base properties of the Na_2O-SiO_2 liquid

Various models of the acid/base properties of glasses are proposed in the literature. The first description was given by Lux in 1939 [17]. This model links the basicity of the liquid to the quantity of "free" oxygen anion O^{2-} ions. The anion quantity results from the dissociation of the alkali oxides in the liquid. Based on the same idea, Toop and Somis have proposed a model in which the O^{2-} are in equilibrium with the bridging and the non-bridging oxygens [18]. Other approaches based on the Pauling electronegativity [19] or the forces of the bounds between the ions [20] also exist. The optical basicity model developed by Duffy [21] is widely used because of its simple calculation. Nevertheless, the thermodynamic approach which considers the "free" oxygen is useful to describe chemical reactions in silica-based liquids. Several measurements of this quantity (usually called the Na_2O activity) using various methods have been reported in the literature. The results obtained for the Na_2O-SiO_2 system by transpiration technic and mass spectroscopy [22–24], electromotive force measurements [25,26] and mixing enthalpy measurements [27,28] give values close to each other (from 10^{-11} to 10^{-5} depending on the temperature and the composition of the liquid).

The approach chosen to describe the acid/base properties of the liquid is based on chemical reactions of the silica network with Na_2O. Such a model has already been presented by Maekawa *et al.* [29]. The basic chemical reactions can be written as follow:

$$Q^n + \frac{1}{2}Na_2O \overset{K_n}{\Leftrightarrow} Q^{n-1} \qquad \text{eq. 1}$$

$$K_n = \frac{a_{Q^{n-1}}}{a_{Q^n} \cdot a_{Na_2O}{}^{1/2}} \qquad \text{eq. 2}$$

In the above equations, Q^n is the classical symbol to design a silica tetrahedron holding n bridging oxygens and a_i is the activity of the chemical species i. In the case of the Na_2O-SiO_2 liquids containing from 20%.mol up to 40%.mol of Na_2O, the main silica tetrahedra are Q^4, Q^3 and Q^2 [29,30], Q^1 and Q^0 being neglectable. The following equation can be derived from the mass balance of SiO_2 and Na_2O and the two mass action laws involving the three main kinds of silica tetrahedra (eq 2), the detail can be found in Appendix A.

$$a_{Na_2O} = \left(\frac{\sqrt{\left(\frac{9}{4}\lambda^2 - \frac{3}{2}\lambda + \frac{1}{4}\right) K_4{}^2 - (8\lambda^2 - 4\lambda)K_4K_3} + \left(\frac{3}{2}\lambda - \frac{1}{2}\right) K_4}{(2 - 4\lambda)K_4K_3} \right)^2 \qquad \text{eq. 3}$$

In this expression, λ is the molar fraction of Na_2O in the soda-silica liquid $(Na_2O)_\lambda(SiO_2)_{1-\lambda}$. The reaction constants K_4 and K_3 of the two chemical reactions (n = 4 and 3) are obtained by fitting the a_{Na_2O} data of Sugawara *et al.* [28] over a temperature range from 900 °C to 1500 °C and for λ ranging from 0.2 to 0.4. The fitted enthalpies and entropies of the reactions considered here are presented in table 1. The Na_2O activity calculated from eq.3 and the polynomial expression proposed by Sugawara *et al.* are presented in figure 1.

3.2. Acid/base and redox reactions of Cr_2O_3 in the Na_2O-SiO_2 system

Solubility and redox (reduction/oxidation) properties of chromium in various glass compositions have been studied by several authors [5,13,14,31–34]. Three oxidation states of the chromium are possible in these media: Cr^{II}, Cr^{III}, Cr^{VI}. The speciation of chromium is due to the acid/base (a_{Na_2O}) and the redox properties of the liquid (O_2 activity in the liquid which is assumed to be in equilibrium with the O_2 pressure in the atmosphere above the melt). Khedim *et al*. have performed solubility measurements of chromium in the Na_2O-SiO_2 system for various compositions, temperatures and oxygen partial pressures [14]. They have proposed three chemical reactions (eq.4 – 6):

$$\frac{1}{2}Cr_2O_{3\,cristal} \overset{dissolution}{\Longleftrightarrow} Cr^{III}O_X^{(3-2X)+} + \left(\frac{3}{2}-X\right)O^{2-} \qquad \text{eq. 4}$$

$$Cr^{III}O_X^{(3-2X)+} + \frac{3}{4}O_2 + \left(Y-X-\frac{3}{2}\right)O^{2-} \overset{oxidation}{\Longleftrightarrow} Cr^{VI}O_Y^{(2Y-6)-} \qquad \text{eq. 5}$$

$$Cr^{III}O_X^{(3-2X)+} \overset{reduction}{\Longleftrightarrow} Cr^{II}O_Z^{(2-2Z)+} + \frac{1}{4}O_2 + \left(X-Z-\frac{1}{2}\right)O^{2-} \qquad \text{eq. 6}$$

In these expressions, X, Y and Z are the apparent oxygen valences of Cr^{III}, Cr^{VI} and Cr^{II} respectively. The O^{2-} activity is assimilated to the Na_2O activity. The associated mass action laws are given below:

$$K_d = a_{Cr^{III}O_X^{(3-2X)+}} \cdot a_{Na_2O}{}^{\left(\frac{3}{2}-X\right)} \qquad \text{eq. 7}$$

$$K_o = \frac{a_{Cr^{VI}O_Y^{(2Y-6)-}}}{a_{Cr^{III}O_X^{(3-2X)+}} \cdot P_{O_2}{}^{3/4} \cdot a_{Na_2O}{}^{\left(Y-X-\frac{3}{2}\right)}} \qquad \text{eq. 8}$$

$$K_r = \frac{a_{Cr^{II}O_Z^{(2Z-2)-}} \cdot P_{O_2}{}^{1/4} \cdot a_{Na_2O}{}^{\left(X-Z-\frac{1}{2}\right)}}{a_{Cr^{III}O_X^{(3-2X)+}}} \qquad \text{eq. 9}$$

In which P_{O_2} is the oxygen partial pressure in the atmosphere above the liquid. The activities of chromium are assimilated to the atomic fractions. The total amount of chromium in the liquid can be derived from the equations 7, 8 and 9:

$$x_{Cr} = K_d \cdot a_{Na_2O}^{\left(X-\frac{3}{2}\right)} \left(1 + K_o \cdot a_{Na_2O}^{\left(Y-X-\frac{3}{2}\right)} {P_{O_2}}^{3/4} + K_r \cdot a_{Na_2O}^{\left(Z+\frac{1}{2}-X\right)} {P_{O_2}}^{-1/4}\right) \qquad \text{eq. 10}$$

In this expression x_{Cr} is the total atomic fraction of chromium. Khedim *et al.* have evaluated the thermodynamic data independently by successive linear fits. In order to obtain more accurate values, the experimental data of solubility are fitted using directly the eq. 10. The adjusted quantities are the three reaction enthalpies, the three reaction entropies and the three oxygen valences for the chromium. The Na_2O activities are calculated from the equation 3. The experimental data from Khedim *et al.* [14] and the values predicted by our model for the $(Na_2O)_{0.25}(SiO_2)_{0.75}$ system after the minimization of the mean square errors are presented in figure 2. The thermodynamic data are given in table 1.

4. Modeling the dissolution of chromia in soda-silica liquids

4.1. Chemical reactions

In the previous sections, 5 chemical reactions (two for the equation 1 and three for the equations 4, 5 and 6) have been identified. Some simplifications are possible to ease the calculation of the reaction rates. Firstly, in most of industrial applications, the atmosphere above the silica-based liquid is air or argon; the oxygen partial pressure is thus high enough to neglect the formation of Cr^{II} (equation 6). Secondly, the Na_2O or O^{2-} activity is extremely low in the studied range of composition (10^{-10} to 10^{-6} according to the previous section). The evolution of concentrations of Na_2O or O^{2-} with time due to the chemical reactions can be relatively fast. In this case, the equations of the reaction rates shall require a thin time mesh in

order to be properly integrated, thus involving a very long time of calculation to make the simulation applicable. The mass action laws can be rewritten in order to eliminate the Na_2O activity from the expression without changing the equilibrium state. This can be done by substituting the Na_2O activity by the Q^n equilibrium (equation 2). Moreover, reaction rates are usually expressed as variations of concentration over time and concentrations are more convenient to use then molar fractions. The simplified mass action laws are rewritten to be expressed as concentration dependent, the conversions are detailed in Appendix B. They correspond to simplified reactions in which the chemical species interact directly with Q^3 and Q^4 instead of Na_2O. Because these simplified reactions are obtained by substitution of Na_2O by the pre-existent Q^3/Q^4 equilibrium, the final equilibrium of the system remains the same.

$$H_{O_2} = \frac{C_{O_2}}{P_{O_2}} \qquad \text{eq. 11}$$

$$K_d' = C_{total} \cdot {K_4}^{(3-2X)} \cdot K_d = \frac{C_{Cr^{III}O_X^{(3-2X)+}} \cdot {C_{Q^3}}^{(3-2X)}}{{C_{Q^4}}^{(3-2X)}} \qquad \text{eq. 12}$$

$$K_o' = {H_{O_2}}^{-3/4} \cdot {K_4}^{-(2Y-2X-3)} \cdot K_o = \frac{C_{Cr^{VI}O_Y^{(2Y-6)-}} \cdot {C_{Q^4}}^{(2Y-2X-3)}}{C_{Cr^{III}O_X^{(3-2X)+}} \cdot {C_{O_2}}^{3/4} \cdot {C_{Q^3}}^{(2Y-2X-3)}} \qquad \text{eq. 13}$$

$$K_s' = K_3 \cdot {K_4}^{-1} = \frac{C_{Q^2} \cdot C_{Q^4}}{{C_{Q^3}}^2} \qquad \text{eq. 14}$$

In the above expressions, K_j' is the equilibrium constant of the simplified reaction j expressed as a function of concentrations, H_{O_2} is the equilibrium constant (in $mol.m^{-3}.atm^{-1}$) between the dissolved oxygen (O_2) in the liquid and the oxygen partial pressure in the atmosphere (Henry constant), C_i is the concentration in $mol.m^{-3}$ of the chemical species i, C_{total} is the total atomic concentration in $mol.m^{-3}$. The elimination of Na_2O activity from the

equilibrium leads to a new equilibrium constant K_s', which corresponds to an equilibrium between Q^4, Q^3 and Q^2. The reaction rates can be written as follow:

$$\xi_d = kc_d \left(K_d' \cdot {C_{Q^4}}^{(3-2X)} - C_{Cr^{III}O_X^{(3-2X)+}} \cdot {C_{Q^3}}^{(3-2X)} \right) \quad \text{eq. 15}$$

$$\xi_o = kc_o \left(K_o' \cdot C_{Cr^{III}O_X^{(3-2X)+}} \cdot {C_{O_2}}^{3/4} \cdot {C_{Q^3}}^{(2Y-2X-3)} - C_{Cr^{VI}O_Y^{(2Y-6)-}} \cdot {C_{Q^4}}^{(2Y-2X-3)} \right) \quad \text{eq. 16}$$

$$\xi_s = kc_s \left(K_s' \cdot {C_{Q^3}}^2 - C_{Q^2} \cdot C_{Q^4} \right) \quad \text{eq. 17}$$

In which ξ_j is the reaction rate of the chemical reaction j (in $mol.m^{-3}.s^{-1}$), kc_j is the reaction rate constant of the chemical reaction j. The thermochemical equilibrium is reached when all the chemical reaction rates are equal to zero. The variation over time of concentration of a chemical species i can be written as follows:

$$\frac{dC_i}{dt} = \sum_j^m v_{i,j} \xi_j \quad \text{eq. 18}$$

In which m is the total amount of chemical reactions. The terms $v_{i,j}$ correspond to the stoichiometric coefficient of the compound i in the reaction j. The $v_{i,j}$ components can be written in a matrix form (i are the chemical compounds and j are the reactions):

$$[v] = \begin{bmatrix} 1 & -1 & 0 \\ 0 & 1 & 0 \\ 1/2 & 0 & 0 \\ 0 & -3/4 & 0 \\ -(3-2X) & (2Y-2X-3) & 1 \\ (3-2X) & -(2Y-2X-3) & -2 \\ 0 & 0 & 1 \\ 0 & 0 & 0 \end{bmatrix} \begin{matrix} \leftarrow C_{Cr^{III}O_X^{(3-2X)+}} \\ \leftarrow C_{Cr^{VI}O_Y^{(2Y-6)-}} \\ \leftarrow Cr_2O_3 \\ \leftarrow O_2 \\ \leftarrow Q^4 \\ \leftarrow Q^3 \\ \leftarrow Q^2 \\ \leftarrow Na^+ \end{matrix} \quad \text{eq. 19}$$

$$\begin{matrix} \uparrow & \uparrow & \uparrow \\ \xi_d & \xi_o & \xi_s \end{matrix}$$

4.2. Mass transport

The mass transport in liquids is expressed with the Nernst-Einstein formalism. The force at the origin of the mass flow is the electrochemical gradient. A convective term is also considered. The flux of a species i is expressed as follows:

$$\vec{J_i} = -\frac{D_i}{RT} C_i \overrightarrow{\nabla \tilde{\mu}_i} + C_i \vec{V} \qquad \text{eq. 20}$$

In which, $\vec{J_i}$ is the flux of the chemical species i (mol.m^{-2}.s^{-1}), D_i is the diffusion coefficient, $\tilde{\mu}_i$ is the electrochemical potential (J.mol^{-1}), $\vec{V}$ is the velocity field of the fluid (m.s^{-1}), R is the gas constant (J.mol^{-1}.K^{-1}) and T the absolute temperature (K). The Onsager theory could be a better formalism [35,36], but the complete kinetic matrix would be complex to determine due to the large number of different chemical species. In the case of oxide layer dissolution, the above equation is defined in the reference frame in which the oxide/liquid interface is fixed in space. The unit vector is oriented from the oxide to the core of the liquid.

By developing the electrochemical potential $\tilde{\mu}_i$ and assuming that the activity is equal or at least proportional to the atomic fraction (ideal or Henry approximation), the complete expression of the mass flow can be formulated as the sum of three components:

$$\vec{J_i} = \overrightarrow{J_i^{Chemical}} + \overrightarrow{J_i^{Electrical}} + \overrightarrow{J_i^{Convective}} \qquad \text{eq. 21}$$

$$\overrightarrow{J_i^{Chemical}} = -D_i \left(\overrightarrow{\nabla C_i} - \frac{C_i}{C_{total}} \overrightarrow{\nabla C_{total}} \right) \qquad \text{eq. 22}$$

$$\overrightarrow{J_i^{Electrical}} = \frac{D_i}{RT} C_i z_i \vec{E} \qquad \text{eq. 23}$$

$$\overrightarrow{J_i^{Convective}} = C_i \vec{V} \qquad \text{eq. 24}$$

Where $\vec{\nabla}$ is the classical derivative operator, z_i is the electric charge of the chemical species i (C.mol^{-1}) and $\vec{E}$ is the electric field in the liquid. The detail of the equation 22 is given in Appendix C. The concentration gradients are known from the initial concentration

distribution, the boundary conditions and the integration of the equation system over time, but $\vec{E}$ and $\vec{V}$ must be calculated from additional conditions.

4.2.1. Electric field

The electric field $\vec{E}$ is calculated in order to ensure the electro-neutrality in the liquid. The convective term $\overrightarrow{J_i^{Convective}}$ cannot generate space charges because the velocity is the same for all chemical species and the chemical reactions conserve intrinsically the mass and charge balances. On the other hand, the chemical flux term $\overrightarrow{J_i^{Chemical}}$ can carry an electric current and thus generate space charges because of the various diffusion coefficients. The electric term $\overrightarrow{J_i^{Electrical}}$ must counterbalance this electric current by satisfying the following equation:

$$\sum_i^n z_i \overrightarrow{J_i^{Electrical}} = -\sum_i^n z_i \overrightarrow{J_i^{Chemical}} \qquad \text{eq. 25}$$

In which, n is the total amount of chemical species. Thus, the following expression of the electric field can be easily derived:

$$\vec{E} = RT \frac{\sum_i^n z_i \overrightarrow{J_i^{Chemical}}}{\sum_i^n z_i^2 D_i C_i} \qquad \text{eq. 26}$$

4.2.2. Velocity field

The velocity field is calculated to ensure the mechanical equilibrium in the liquid. The molar volume of the liquid is postulated to be a linear combination of the molar volume of each oxide weighted by molar fraction in the liquid. A deviation of the molar volume of the liquid involves an increase of the pressure and reciprocally. The dimensionless quantity called normalized volume is defined as follows:

$$\hat{v} = \sum_{i}^{n} V_{m_i} C_i \qquad \text{eq. 27}$$

In which $\hat{v}$ is the normalized volume and V_{m_i} is the molar volume of the chemical species i ($m^3.mol^{-1}$). This quantity is equal to 1 when the liquid is at the mechanical equilibrium (no pressure in the liquid). The following expression corresponds to the conservation law applied to the normalized volume:

$$\frac{\partial \hat{v}}{\partial t} + \vec{\nabla} \cdot (\hat{v}\, \vec{V}) = \tau_{\hat{v}} \qquad \text{eq. 28}$$

The velocity field $\vec{V}$ appears in the above equation. The term $\tau_{\hat{v}}$ is the production rate of the normalized volume (s^{-1}). This quantity must take into account each chemical reaction or mass flow that could lead to a variation of the normalized volume:

$$\tau_{\hat{v}} = \sum_{i}^{n} V_i^m \left(\vec{\nabla} \cdot \left(\overrightarrow{J_i^{Chemical}} + \overrightarrow{J_i^{Electrical}} \right) + \sum_{j}^{m} v_{i,j} \xi_j \right) \qquad \text{eq. 29}$$

As in the previous equations, i and j correspond to the chemical species and to the chemical reactions respectively. The expression for the velocity field can be obtained by imposing the time derivative of the normalized volume equal to zero in the equation 28:

$$\vec{\nabla} \cdot \vec{V} = \frac{\sum_{i}^{n} V_{m_i} \left(\vec{\nabla} \cdot \left(\overrightarrow{J_i^{Chemical}} + \overrightarrow{J_i^{Electrical}} \right) + \sum_{j}^{m} v_{i,j} \xi_j \right)}{\sum_{i}^{n} V_{m_i} C_i} \qquad \text{eq. 30}$$

4.3. Equations and boundary conditions

4.3.1. Equations

The various physical and chemical phenomena developed in the previous section lead to a system of 8 partial differential equations (equation 31), one integral over space (calculation of the velocity field equation 30) and one simple relation (electric field equation 26)

describing the evolution of the chemical species concentrations in the Na_2O-SiO_2 liquid in interaction with Cr_2O_3. These equations are obtained from the classical conservation law applied to the mass flows of the 8 chemical species ($Cr^{III}O_X^{(3-2X)+}$, $Cr^{VI}O_Y^{(2Y-6)-}$, Cr_2O_3, O_2, Q^4, Q^3, Q^2, Na^+) and the 3 chemical reactions (equation 15 – 17):

$$\frac{\partial C_i}{\partial t} = \vec{\nabla} \cdot \left(\overrightarrow{J_i^{Chemical}} + \overrightarrow{J_i^{Electrical}} + \overrightarrow{J_i^{Convective}} \right) + \sum_j^m v_{i,j} \xi_j \qquad \text{eq. 31}$$

4.3.2. Boundary and initial conditions

The equations are solved over a simple finite one dimensional domain. The chromia and the liquid are in contact at the position x=0. The liquid cannot penetrate the chromia, so the flow of each chemical species across this boundary is null. At the other boundary, the concentrations are constant and equal to the initial values (at t = 0). The length of the domain remains constant during the calculation. The recession of chromia due to its dissolution is implicitly taken into account in the calculation of the velocity field.

The liquid is initially composed of Na^+, O_2 , Q^4, Q^3 and Q^2. The distribution of the silica tetrahedra is given by the molar fraction of Na_2O (λ), equations 2, 3 and the mass balance of silica. As an example, the liquid $(Na_2O)_{0.25}(SiO_2)_{0.75}$ at a temperature of 1150°C has a pNa_2O equal to 9.08 and a distribution of silica tetrahedra corresponding to $Q^4_{0.382}Q^3_{0.569}Q^2_{0.049}$; the total concentration of silicon tetrahedra being equal to the concentration of SiO_2 in the liquid.

The concentration of dissolved oxygen is given by the Henry constant and the external oxygen pressure (equation 11). The liquid is then defined as $Na_2O_{\chi}SiO_{2\,\gamma}O_{2\,\zeta}$; the relations between χ, γ, ζ and the known values of λ, H_{O_2}, P_{O_2} are given in equation 32, 33 and 34 (see Appendix D):

$$\zeta = \frac{H_{O_2} P_{O_2} \left(\frac{\lambda}{1-\lambda} V_{m Na_2O} + V_{m SiO_2} \right)}{1 - H_{O_2} P_{O_2} V_{m O_2}} \gamma \qquad \text{eq. 32}$$

$$\chi = \frac{\lambda}{1-\lambda} \gamma \qquad \text{eq. 33}$$

$$\gamma = \left(\frac{1}{1-\lambda} + \frac{H_{O_2} P_{O_2} \left(\frac{\lambda}{1-\lambda} V_{m Na_2O} + V_{m SiO_2} \right)}{1 - H_{O_2} P_{O_2} V_{m O_2}} \right)^{-1} \qquad \text{eq. 34}$$

A $(Na_2O)_{0.25}(SiO_2)_{0.75}$ liquid with a Henry constant H_{O_2} equal to 2000 mol.m^{-3}.atm^{-1} in air (P_{O_2}=0.2 atm) is written as $(Na_2O)_{0.247}(SiO_2)_{0.742}(O_2)_{0.011}$ with data from table 2. The presence of dissolved oxygen does not affect the distribution of silica tetrahedron. The concentration of Na_2O and the total concentration of SiO_2 can be easily calculated from the above equations and from the molar volume of the liquid $V_{m Liquid}$ (equation 35):

$$V_{m Liquid} = \chi V_{m Na_2O} + \gamma V_{m SiO_2} + \zeta V_{m O_2} \qquad \text{eq. 35}$$

The concentrations of Na^+, O_2 , Q^4, Q^3 and Q^2 at the initial time are then obvious. The liquid is also at the mechanical equilibrium as defined in section 4.2.2. (equation 27 is equal to 1).

5. Results

The simulations were performed with input data from tables 1 and 2 for a $(Na_2O)_{0.25}(SiO_2)_{0.75}$ liquid at 1150°C. The kinetic coefficients of the reactions have been chosen in order to quickly reach the thermochemical equilibrium. The equations system was solved using the finite volume formalism and integrated over time with a simple Euler explicit method [37]. The space mesh so as the integration time step were studied to obtain the more stable and accurate results (a relative tolerance of 10^{-6}, an absolute tolerance of 10^{-4} mol.m^{-3} and a maximum time step of 10^{-4} s). The MATLAB code used to solve the equation system is available in ref [38].

The results of the simulation for 3600 seconds of reaction and the experimental results are presented in figure 3. The unknown Henry constant (H_{O_2}) was adjusted to fit the solubility of the chromium, a value of 2000 $mol.m^{-3}.atm^{-1}$ was found. This is coherent with the estimation from the literature for oxygen [39] or nitrogen [40] in liquid slags. The simulation and the experiment are in good agreement for the diffusion of the chromium. The experimental measurements of Na_2O and SiO_2 concentration profiles are dispersed but consistent with the simulation.

The simulation shows an interdiffusion between the three oxides. The multi-component interdiffusion is usually attributed to cross-diffusion due to non-diagonal terms in the diffusion matrix [12,41,42]. In the present model, the chemical diffusion is only described by a unique diffusion coefficient and the liquid is described as an ideal mix of chemical species. The only possible sources of interdiffusion are the velocity field (equation 30) and the migration due to the electric field (equation 26). In the Onsager formalism, each thermodynamic force can yield a mass flow [35,36] (each chemical potential gradients, the pressure gradient and the electric potential gradient). The kinetic matrix is the proportionality factor between fluxes and forces. The diffusion matrix is a simplification of the Onsager coefficients matrix when the only thermodynamic forces are the chemical potential gradients. In the present model, the influence of the electric field and the velocity field on the diffusion can be analyzed since the equation 23 and 24 give the relation between the fluxes and these two quantities. This analysis is better detailed for chromium diffusion in section 6.3, but silicon and sodium diffusion can be stated: the electro-neutrality condition has a significant influence on the diffusion of ions with high diffusivity such as sodium and the mechanical equilibrium condition influences the diffusion of low diffusivity net-work formers such as silica. The equations 26 and 30 could be used in order to uncouple these two phenomena from the multicomponent interdiffusion in further studies.

The repartition of the Cr^{III}, Cr^{VI} and the dissolved oxygen are presented in figure 4. The oxygen is expressed as the external partial pressure. A decrease of the oxygen pressure towards the liquid/chromia interface can be noticed. This can be explained by the oxidation of the Cr^{III} into Cr^{VI} what consumes the dissolved oxygen in the liquid. The total concentration of chromium at the liquid/chromia interface is imposed by the oxygen pressure. In this simulation the oxygen pressure of 0.093 atmospheres and the total atomic fraction of chromium of 0.82 % (0.38 % Cr^{III} and 0.44 % Cr^{VI}) correspond to the thermodynamic equilibrium [14].

The distribution of the Q^n and the resulting pNa_2O are presented in figure 5. The glass structure is poorly affected by the dissolution of the chromia. The pNa_2O exhibits a slight variation with a higher Na_2O activity close to the liquid/chromia interface due to the dissolution of chromia which yields "free oxygen" in the liquid and a lower Na_2O activity at 100 µm of the interface because of the oxidation of Cr^{III} into Cr^{VI}. The acid/base property of the liquid can be considered as unchanged by the dissolution of chromia. This affirmation is only verified for this specific case.

6. Discussion

6.1. Parabolic dissolution regime

The reaction rate constants kc_d, kc_o, kc_s were chosen in order to quickly reach the chemical equilibrium in the liquid. In the present simulation, the equilibrium is reached fast enough to consider that the system is at the thermochemical equilibrium at each point of the space. As an example, the concentrations at the liquid/chromia interface evolve during 10 seconds before reaching their equilibrium values. The diffusion profiles of chromium and oxygen for various times are presented in figure 6. The concentrations remain constant at the liquid/chromia interface and the evolution of the concentrations in the liquid can be

assimilated to classical diffusion profiles for semi-infinite diffusion. Thus, the dissolution rate of chromia can be described by only the solubility and the apparent diffusion coefficient of chromium in the liquid [5,43,44]. The parameters influencing these two quantities are discussed in the last paragraph of this section. The dissolution rate of the oxide obeys the following parabolic law.

$$\frac{de}{dt} = -\frac{V_{m_{Cr_2O_3}}}{2} S_{Cr} \sqrt{\frac{D_{Cr}^{App}}{\pi t}} = -\sqrt{\frac{k_d}{2t}} \qquad \text{eq. 36}$$

In this expression, e is the thickness of the oxide in m, $V_{m_{Cr_2O_3}}$ is the molar volume of chromia, S_{Cr} is the concentration of chromium at the liquid/oxide interface in mol.m^{-3} (i.e. solubility limit), D_{Cr}^{App} is the apparent diffusion coefficient of the chromium in the liquid in m².s^{-1} and k_d is the parabolic dissolution constant in m².s^{-1}. In the presented simulation, D_{Cr}^{App} was found to be 1 10^{-12} m².s^{-1} (this parameter is different from the true diffusion coefficient of Cr^{III} and Cr^{IV} used for this calculation), S_{Cr} is equal to 901 mol.m^{-3} (0.82% atomic fraction) and the parabolic dissolution rate is 1.15 10^{-16} m².s^{-1}. These values and the equation 36 fit the recession rate of the oxide presented in figure 7 with $R^2 = 0.99$.

6.2. Interface recession and velocity field

The problem of the moving boundary is usually encountered in materials chemistry because of the recession of an interface due to the consumption of the material. This can have a significant effect on the evolution of the considered reaction [45]. This aspect has not been explained in the presented model. The position x = 0 corresponds to the liquid/oxide interface in the referential in which the equations are solved. The referential can be seen as moving from the perspective of the initial referential (t = 0). This velocity is equivalent to the velocity field calculated with the equation 30. From the perspective of our referential in which the liquid/chromia interface is fixed in space, the dissolved chromia must occupy a new volume

in the liquid. In order to achieve that, the liquid is pushed by the incoming matter yielding a velocity. This is encoded in the equation 30 in which this principle is generalized to the diffusion and chemical reactions.

The evolution of the velocity field at different positions and times in the liquid is presented in figure 8. By convention, the positive values correspond to a vector oriented along x axis. The intensity of the velocity field is time dependent, but its orientation does not change. Close to the liquid/chromia interface, the velocity increases due to the diffusion of sodium and silica towards the position x = 0. The velocity converges to a time dependent value far from the interface; this value corresponds to the recession of the oxide. The velocity at the position x = 500 µm and the recession rate of the oxide are presented in figure 7; the two values are proportional. The reason of this proportionality, and not the equality, is the oxidation of chromium III in chromium VI in the liquid. Because of the higher molar volume of Cr^{VI} set in the simulation (table 2), the dissolved chromia occupies slightly more space in the liquid than the space it occupies in the oxide layer.

6.3. Phenomena influencing the dissolution rate of chromia

Among the various phenomena highlighted in this paper, only a few seem to have a significant influence on the dissolution rate of the chromia in the silica-based liquid. The velocity field studied in the above section brings a low contribution to the diffusion of the chromium. After the 3600 seconds of simulation, the diffusion profile of chromium spreads over 200 µm while the displacement due to the velocity field is 1 µm. The electric field in the liquid is presented in figure 9; the convention for the vector field is the same as the one used for the velocity field. The value of this field is several decades of $V.m^{-1}$. The velocity of the Cr^{VI} with its high electric charge can be calculated with the Nernst-Einstein equation. For an electric field of 50 $V.m^{-1}$ the velocity of the Cr^{VI} ion (as defined in table 2) at a temperature of 1150 °C is around 1.3 10^{-10} $m.s^{-1}$, which is lower than the total velocity field. Then, both

electric and velocity field have a negligible effect on the diffusion of the chromium in the liquid.

On the other hand, the oxygen pressure and diffusion in the liquid seem to have a significant influence on the dissolution rate of the chromia. As explained, the dissolution of chromia can be described by the solubility of chromium and its apparent diffusion coefficient. The solubility of chromium depends on the acid/base properties of the liquid and the oxygen pressure at the liquid/chromia interface. The last quantity is directly related to the concentration/partial pressure of oxygen, its diffusion coefficient and the diffusion coefficients of chromium. Moreover, the evolution of the oxygen partial pressure in the liquid affects the Cr^{VI}/Cr^{III} ratio. It is possible to prove that the apparent diffusion coefficient of the chromium (D_{Cr}^{App}) can be written as follows (details in Appendix E):

$$D_{Cr}^{App} = \left(P + \frac{\partial P}{\partial C_{Cr}^{App}} C_{Cr}^{App} \right) D_{Cr^{III}} + \left(1 - P - \frac{\partial P}{\partial C_{Cr}^{App}} C_{Cr}^{App} \right) D_{Cr^{VI}} \qquad \text{eq. 37}$$

In the above expression, P is the fraction of Cr^{III} among the total chromium concentration, noted here as C_{Cr}^{App}. From figure 4, it can be deduced that P is slightly lower than 0.5 for this simulation. The application of equation 37 with a constant P value of 0.5 leads to a D_{Cr}^{App} of 10^{-12} $m^2.s^{-1}$, which is the value obtained by fitting the simulated profile of chromium with the classical erfc function or the value obtain from the dissolution rate of chromia (section 6.1.). Thus, the apparent diffusion coefficient can vary between the diffusion coefficients of Cr^{III} and Cr^{VI}. It appears that the model could be reduced to a system containing only Cr^{III}, Cr^{VI} and O_2 for studying the corrosion of chromia-forming alloy in silica-based liquids.

7. Conclusions

A model of the dissolution of chromia in Na_2O-SiO_2 liquids has been developed. The aim was to formulate a model as complete as possible taking into account the physical and chemical phenomena occurring in that kind of interaction. Results from the literature were used in order to determine the thermodynamic data required for simulating the dissolution of chromia in silica-based liquids.

The equation system of the model has been solved with a numerical method. The simulation and the experimental results are in good agreement despite the dispersion of the Na_2O and SiO_2 measurements. The model predicts the interdiffusion of the three oxides. The electro-neutrality and mechanical equilibrium principals implemented in the model are at the origin of the interdiffusion. The model reveals that the acid/base property of the liquid is not much affected by the dissolution of the chromia. The oxidation of chromium III into chromium VI in the liquid consumes a part of the dissolved oxygen affecting the speciation and diffusion of chromium. It has been proved that the moving boundary due to the recession of the oxide during its dissolution is intrinsically considered without using re-meshing methods.

The use of such a model for corrosion application is also debated. Since the basicity of the liquid is not affected by the dissolution of chromium, the chemical reactions can be simplified by considering a constant Na_2O activity. The velocity and the electric field have a negligible effect on the dissolution of chromia. Under certain conditions, it seems that the model can be reduced to the simple diffusion of Cr^{III}, Cr^{VI} and O_2 and the oxidation reaction of Cr^{III}.

Acknowledgements

The authors wish to thank the « Centre de Compétences en Microscopies, Microsondes et Métallographie » of the Jean Lamour Institute for providing the technical support for the EPMA presented in this work.

The authors also wish to thank Jean- Marc Commenge from the LRGP (Laboratoire Réaction et Génie des Procédés), Francis Kosior from the Jean Lamour institute and Gerald Monard from the LCPT (Laboratoire de Chimie et Physique Théorique) for their advice concerning numerical simulations.

References

[1] P. Sengupta, Interaction study between nuclear waste-glass melt and ceramic melter bellow liner materials, J. Nucl. Mater. 411 (2011) 181–184. https://doi.org/10.1016/j.jnucmat.2011.01.122.

[2] J. Di Martino, C. Rapin, P. Berthod, R. Podor, P. Steinmetz, Corrosion of metals and alloys in molten glasses. Part 1: glass electrochemical properties and pure metal (Fe, Co, Ni, Cr) behaviours, Corros. Sci. 46 (2004) 1849–1864. https://doi.org/10.1016/j.corsci.2003.10.024.

[3] J. Di Martino, C. Rapin, P. Berthod, R. Podor, P. Steinmetz, Corrosion of metals and alloys in molten glasses. Part 2: nickel and cobalt high chromium superalloys behaviour and protection, Corros. Sci. 46 (2004) 1865–1881. https://doi.org/10.1016/j.corsci.2003.10.025.

[4] L.J. Manfredo, R.N. McNally, Solubility of Refractory Oxides in Soda-Lime Glass, J. Am. Ceram. Soc. 67 (1984) C-155-C–158. https://doi.org/10.1111/j.1151-2916.1984.tb19178.x.

[5] E. Schmucker, C. Petitjean, P.-J. Panteix, L. Martinelli, S. Ben Lagha, M. Vilasi, Correlation between chromium physicochemical properties in silicate melts and the corrosion behavior of chromia-forming alloy, J. Nucl. Mater. 510 (2018) 100–108. https://doi.org/10.1016/j.jnucmat.2018.07.059.

[6] C. Rüssel, Self diffusion of polyvalent ions in a soda-lime-silica glass melt, J. Non-Cryst. Solids. 134 (1991) 169–175. https://doi.org/10.1016/0022-3093(91)90025-2.

[7] O. Clauβen, C. Rüssel, Self diffusion of polyvalent ions in a borosilicate glass melt, J. Non-Cryst. Solids. 215 (1997) 68–74. https://doi.org/10.1016/S0022-3093(97)00036-7.

[8] O. Clauβen, Diffusivities of polyvalent elements in glass melts, Solid State Ion. 105 (1998) 289–296. https://doi.org/10.1016/S0167-2738(97)00476-1.

[9] O. Clauβen, S. Gerlach, C. Rüssel, Self-diffusivity of polyvalent ions in silicate liquids, J. Non-Cryst. Solids. 253 (1999) 76–83. https://doi.org/10.1016/S0022-3093(99)00345-2.

[10] J. Horbach, W. Kob, K. Binder, Structural and dynamical properties of sodium silicate melts: an investigation by molecular dynamics computer simulation, Chem. Geol. 174 (2001) 87–101. https://doi.org/10.1016/S0009-2541(00)00309-0.

[11] M. Bauchy, B. Guillot, M. Micoulaut, N. Sator, Viscosity and viscosity anomalies of model silicates and magmas: A numerical investigation, Chem. Geol. 346 (2013) 47–56. https://doi.org/10.1016/j.chemgeo.2012.08.035.

[12] H. Pablo, S. Schuller, M.J. Toplis, E. Gouillart, S. Mostefaoui, T. Charpentier, M. Roskosz, Multicomponent diffusion in sodium borosilicate glasses, J. Non-Cryst. Solids. 478 (2017) 29–40. https://doi.org/10.1016/j.jnoncrysol.2017.10.001.

[13] H. Khedim, R. Podor, C. Rapin, M. Vilasi, Redox-Control Solubility of Chromium Oxide in Soda-Silicate Melts, J. Am. Ceram. Soc. 91 (2008) 3571–3579. https://doi.org/10.1111/j.1551-2916.2008.02692.x.

[14] H. Khedim, R. Podor, P.J. Panteix, C. Rapin, M. Vilasi, Solubility of chromium oxide in binary soda-silicate melts, J. Non-Cryst. Solids. 356 (2010) 2734–2741. https://doi.org/10.1016/j.jnoncrysol.2010.09.045.

[15] E. Schmucker, C. Petitjean, L. Martinelli, P.-J. Panteix, S. Ben Lagha, M. Vilasi, Oxidation of Ni-Cr alloy at intermediate oxygen pressures. I. Diffusion mechanisms through the oxide layer, Corros. Sci. 111 (2016) 474–485. https://doi.org/10.1016/j.corsci.2016.05.025.

[16] E. Schmucker, C. Petitjean, L. Martinelli, P.-J. Panteix, B. Lagha, M. Vilasi, Oxidation of Ni-Cr alloy at intermediate oxygen pressures. II. Towards the lifetime prediction of alloys, Corros. Sci. 111 (2016) 467–473. https://doi.org/10.1016/j.corsci.2016.05.024.

[17] H. Lux, “Säuren” und “Basen” im Schmelzfluss: Die Bestimmung der Sauerstoffionen-Konzentration, Z. Für Elektrochem. Angew. Phys. Chem. 45 (1939) 303–309. https://doi.org/10.1002/bbpc.19390450405

[18] G.W. Toop, C.S. Somis, Some New Ionic Concepts of Silicate Slags, Can. Metall. Q. 1 (1962) 129–152. https://doi.org/10.1179/cmq.1962.1.2.129.

[19] R.T. Sanderson, Electronegativities in inorganic chemistry, J. Chem. Educ. 29 (1952) 539. https://doi.org/10.1021/ed029p539.

[20] K. Sun, A scale of acidity and basicity in glass, Glass Ind. 29 (1948) 73–74.

[21] J.A. Duffy, A review of optical basicity and its applications to oxidic systems, Geochim. Cosmochim. Acta. 57 (1993) 3961–3970. https://doi.org/10.1016/0016-7037(93)90346-X.

[22] D.N. Rego, G.K. Sigworth, W.O. Philbrook, Thermodynamic study of Na_2O-SiO_2 melts at 1300° and 1400 °C, Metall. Trans. B. 16 (1985) 313–323. https://doi.org/10.1007/BF02679722.

[23] R. Chastel, C. Bergman, J. Rogez, J.-C. Mathieu, Excess thermodynamic functions in ternary Na_2O-K_2O-SiO_2 melts by Knudsen cell mass spectrometry, Chem. Geol. 62 (1987) 19–29. https://doi.org/10.1016/0009-2541(87)90053-2.

[24] A.I. Zaitsev, N.E. Shelkova, B.M. Mogutnov, Thermodynamics of Na_2O-SiO_2 melts, Inorg. Mater. 36 (2000) 529–543. https://doi.org/10.1007/BF02757949.

[25] D.A. Neudorf, J.F. Elliott, Thermodynamic properties of Na_2O-SiO_2-CaO melts at 1000 to 1100 °C, Metall. Trans. B. 11 (1980) 607–614. https://doi.org/10.1007/BF02670140.

[26] H. Itoh, T. Yokokawa, Thermodynamic activity of Na_2O in Na_2O–SiO_2–Al_2O_3 melt, Trans. Jpn. Inst. Met. 25 (1984) 879–884. https://doi.org/10.2320/matertrans1960.25.879.

[27] F. Tsukihashi, N. Sano, Measurement of the Activity of Na_2O in Na_2O-SiO_2 Melts by Chemical Equilibration Method, Tetsu--Hagane. 71 (1985) 815–822. https://doi.org/10.2355/tetsutohagane1955.71.7_815.

[28] T. Sugawara, K. Shinoya, S. Yoshida, J. Matsuoka, Thermodynamic mixing properties of liquids in the system Na_2O-SiO_2, J. Non-Cryst. Solids. 357 (2011) 1390–1398. https://doi.org/10.1016/j.jnoncrysol.2010.09.064.

[29] H. Maekawa, T. Maekawa, K. Kawamura, T. Yokokawa, The structural groups of alkali silicate glasses determined from 29Si MAS-NMR, J. Non-Cryst. Solids. 127 (1991) 53–64. https://doi.org/10.1016/0022-3093(91)90400-Z.

[30] W.E. Halter, B.O. Mysen, Melt speciation in the system Na_2O–SiO_2, Chem. Geol. 213 (2004) 115–123. https://doi.org/10.1016/j.chemgeo.2004.08.036.

[31] T.K. Abdullah, C. Petitjean, P.-J. Panteix, C. Rapin, M. Vilasi, Z. Hussain, A. Abdul Rahim, Dissolution equilibrium of chromium oxide in a soda lime silicate melt exposed to oxidizing and reducing atmospheres, Mater. Chem. Phys. 142 (2013) 572–579. https://doi.org/10.1016/j.matchemphys.2013.07.055.

[32] A.J. Berry, H.St.C. O'Neill, D.R. Scott, G.J. Foran, J.M.G. Shelley, The effect of composition on Cr^{2+}/Cr^{3+} in silicate melts, Am. Mineral. 91 (2006) 1901–1908. https://doi.org/10.2138/am.2006.2097.

[33] C.-W. Kim, K. Choi, J.-K. Park, S.-W. Shin, M.-J. Song, Enthalpies of Chromium Oxide Solution in Soda Lime Borosilicate Glass Systems, J. Am. Ceram. Soc. 84 (2001) 2987–2990. https://doi.org/10.1111/j.1151-2916.2001.tb01125.x.

[34] P.L. Roeder, I. Reynolds, Crystallization of Chromite and Chromium Solubility in Basaltic Melts, J. Petrol. 32 (1991) 909–934. https://doi.org/10.1093/petrology/32.5.909.

[35] L. Onsager, Reciprocal Relations in Irreversible Processes. I., Phys. Rev. 37 (1931) 405–426. https://doi.org/10.1103/PhysRev.37.405.

[36] L. Onsager, Reciprocal Relations in Irreversible Processes. II., Phys. Rev. 38 (1931) 2265–2279. https://doi.org/10.1103/PhysRev.38.2265.

[37] W.H. Press, Numerical recipes: the art of scientific computing, Cambridge University Press, Cambridge, UK; New York, 2007.

[38] V. Szczepan, Data for: A new modeling of the dissolution of chromia in Na_2O-SiO_2 liquids, 1 (2020). https://doi.org/10.17632/wnytyxc4wv.1.

[39] M. Sasabe, K.S. Goto, Permeability, diffusivity, and solubility of oxygen gas in liquid slag, Metall. Trans. 5 (1974) 2225–2233. https://doi.org/10.1007/BF02643937.

[40] H.-O. Mulfinger, Physical and Chemical Solubility of Nitrogen in Glass Melts, J. Am. Ceram. Soc. 49 (1966) 462–467. https://doi.org/10.1111/j.1151-2916.1966.tb13300.x.

[41] C. Guo, Y. Zhang, Multicomponent diffusion in basaltic melts at 1350 °C, Geochim. Cosmochim. Acta. 228 (2018) 190–204. https://doi.org/10.1016/j.gca.2018.02.043.

[42] C. Claireaux, M.-H. Chopinet, E. Burov, H. Montigaud, M. Roskosz, M.J. Toplis, E. Gouillart, Influence of temperature on multicomponent diffusion in calcium and sodium aluminosilicate melts, J. Non-Cryst. Solids. 505 (2019) 170–180. https://doi.org/10.1016/j.jnoncrysol.2018.09.046.

[43] T. Gheno, B. Gleeson, Kinetics of Al_2O_3-Scale Growth by Oxidation and Dissolution in Molten Silicate, Oxid. Met. 87 (2017) 527–539. https://doi.org/10.1007/s11085-016-9686-0.

[44] T. Gheno, G. Lindwall, On the Simulation of Composition Profiles in NiCoCrAl Alloys During Al_2O_3 Scale Growth in Oxidation and Oxidation–Dissolution Regimes, Oxid. Met. 91 (2019) 243–257. https://doi.org/10.1007/s11085-018-9877-y.

[45] C. Wagner, Theoretical Analysis of the Diffusion Processes Determining the Oxidation Rate of Alloys, J. Electrochem. Soc. 99 (1952) 369. https://doi.org/10.1149/1.2779605.

Figure captions

Fig. 1. Evolution of pNa_2O with the composition of the binary system Na_2O-SiO_2 according to the data from Sugawara *et al.* [28] (red dots) and the presented model (black lines) after minimization of the mean square errors.

Fig. 2. Evolution of the solubility of chromium with the oxygen fugacity in the $(Na_2O)_{0.25}(SiO_2)_{0.75}$ liquid according to the data from Khedim *et al.* [14] (red dots) and the presented model (black lines) after minimization of the mean square errors over the solubility data.

Fig. 3. EPMA measurements and simulation of the diffusion profile of chromium and the evolution of the melt composition after 1 hour of immersion of the pre-oxidized Ni-30Cr alloy at 1150 °C in $(Na_2O)_{0.25}(SiO_2)_{0.75}$. Si, Na and Cr are expressed in term of the oxides SiO_2, Na_2O and Cr_2O_3 respectively.

Fig. 4. Simulated concentration profiles of Cr^{III}, Cr^{VI} and O_2 in $(Na_2O)_{0.25}(SiO_2)_{0.75}$ at 1150 °C after 1 hour of immersion of the pre-oxidized Ni-30Cr alloy.

Fig. 5. Simulated Q^n ratio and pNa_2O versus the distance from the chromia/liquid interface in $(Na_2O)_{0.25}(SiO_2)_{0.75}$ at 1150 °C after 1 hour of immersion of chromia.

Fig. 6. Simulated concentration profiles of Cr and O_2 in $(Na_2O)_{0.25}(SiO_2)_{0.75}$ at 1150 °C for various immersion duration of the pre-oxidized Ni-30Cr alloy.

Fig. 7. Velocity of the liquid and recession rate of chromia versus time for various distances from the chromia/liquid interface in $(Na_2O)_{0.25}(SiO_2)_{0.75}$ at 1150 °C.

Fig. 8. Velocity of the liquid versus the distance to the chromia/liquid interface in $(Na_2O)_{0.25}(SiO_2)_{0.75}$ at 1150 °C for various immersion duration of the pre-oxidized Ni-30Cr alloy.

Fig. 9. Electric field in the liquid versus the distance from the chromia/liquid interface in $(Na_2O)_{0.25}(SiO_2)_{0.75}$ at 1150 °C for various immersion duration of the pre-oxidized Ni-30Cr alloy.

Appendix A

Equation 3

For a binary liquid defined as $Na_2O_{\lambda}SiO_{2\ 1-\lambda}$, the mass balances on Na_2O and SiO_2 are written as a function of Q^n. If $Q^{0\text{-}1}$ and the free Na_2O are present in low quantity, the mass balances can be written as:

$$x_{Q^4} + x_{Q^3} + x_{Q^2} = 1 - \lambda \quad \text{A. 1}$$

$$\frac{1}{2}x_{Q^3} + x_{Q^2} = \lambda \quad \text{A. 2}$$

With x_{Q^n} the molar fraction of Q^n. The equation A. 1 and A. 2 correspond respectively to the mass balance of SiO_2 and Na_2O. By introducing the equilibrium between Q^n, $Q^{n\text{-}1}$ and Na_2O (equation 1 and 2), equation A. 1 and A. 2 can be written as a function of Na_2O activity (by assuming that the Q^n activity and molar fraction are equivalent:

$$x_{Q^4} + x_{Q^4}K_4 a_{Na_2O}{}^{1/2} + x_{Q^4}K_4K_3 a_{Na_2O} = 1 - \lambda \quad \text{A. 3}$$

$$\frac{1}{2}x_{Q^4}K_4 a_{Na_2O}{}^{1/2} + x_{Q^4}K_4K_3 a_{Na_2O} = \lambda \quad \text{A. 4}$$

By factorization and division, one can obtain the following polynomial expression.

$$(2\lambda - 1)K_4K_3 a_{Na_2O} + \left(\frac{3}{2}\lambda - \frac{1}{2}\right)K_4 a_{Na_2O}{}^{1/2} + \lambda = 0 \quad \text{A. 5}$$

The Na_2O activity is obtained by solving the above equation, which gives equation 3.

$$a_{Na_2O}{}^{1/2} = \frac{\sqrt{\left(\frac{9}{4}\lambda^2 - \frac{3}{2}\lambda + \frac{1}{4}\right)K_4{}^2 - (8\lambda^2 - 4\lambda)K_4K_3} + \left(\frac{3}{2}\lambda - \frac{1}{2}\right)K_4}{(2 - 4\lambda)K_4K_3} \quad \text{A. 5}$$

Appendix B

Conversion of the equilibrium constants

The aim is to convert the equilibrium constants expressed in term of activity into equilibrium constants expressed in term of concentrations and to eliminate the Na_2O activity from the expressions.

The Na_2O activity can be replaced by the Q^4/Q^3 equilibrium and because of the approximation of ideal mixing, the ratio of Q^n activity or concentration are equal.

$$a_{Na_2O} = \frac{{C_{Q^3}}^2}{{K_4}^2 \cdot {C_{Q^4}}^2} \qquad \text{B. 1}$$

Application to K_d

$$K_d = a_{Cr^{III}O_x^{(3-2X)+}} \cdot {a_{Na_2O}}^{\left(\frac{3}{2}-X\right)} \qquad \text{B. 2}$$

The equilibrium constant K_d can thus be written as:

$$K_d = a_{Cr^{III}O_x^{(3-2X)+}} \cdot \frac{{C_{Q^3}}^{(3-2X)}}{{K_4}^{(3-2X)} \cdot {C_{Q^4}}^{(3-2X)}} \qquad \text{B. 3}$$

The $a_{Cr^{III}O_x^{(3-2X)+}}$ corresponds to the atomic fraction of Cr^{III}, K_d can be written as:

$$K_d = \frac{C_{Cr^{III}O_x^{(3-2X)+}}}{C_{total}} \cdot \frac{{C_{Q^3}}^{(3-2X)}}{{K_4}^{(3-2X)} \cdot {C_{Q^4}}^{(3-2X)}} \qquad \text{B. 4}$$

By keeping the concentration on one side of the equality, the new equilibrium constant K_d' appears obvious.

$$K_d' = C_{total} \cdot {K_4}^{(3-2X)} \cdot K_d = \frac{C_{Cr^{III}O_x^{(3-2X)+}} \cdot {C_{Q^3}}^{(3-2X)}}{{C_{Q^4}}^{(3-2X)}} \qquad \text{B. 5}$$

Application to K_o

$$K_o = \frac{a_{Cr^{VI}O_Y^{(2Y-6)-}}}{a_{Cr^{III}O_x^{(3-2X)+}} \cdot {P_{O_2}}^{3/4} \cdot {a_{Na_2O}}^{\left(Y-X-\frac{3}{2}\right)}} \qquad \text{B. 6}$$

The same procedure applied to K_o gives.

$$K_o = \frac{C_{Cr^{VI}O_Y^{(2Y-6)-}} \cdot {C_{Q^4}}^{(2Y-2X-3)} \cdot {K_4}^{(2Y-2X-3)}}{C_{Cr^{III}O_x^{(3-2X)+}} \cdot {P_{O_2}}^{3/4} \cdot {C_{Q^4}}^{(2Y-2X-3)}} \qquad \text{B. 7}$$

With the Henry constant, P_{O_2} can be changed by the oxygen concentration.

$$K_o = \frac{C_{Cr^{VI}O_Y^{(2Y-6)-}} \cdot {H_{O_2}}^{3/4} \cdot {C_{Q^4}}^{(2Y-2X-3)} \cdot {K_4}^{(2Y-2X-3)}}{C_{Cr^{III}O_x^{(3-2X)+}} \cdot {C_{O_2}}^{3/4} \cdot {C_{Q^4}}^{(2Y-2X-3)}} \qquad \text{B. 8}$$

$$K_o' = {H_{O_2}}^{-3/4} \cdot {K_4}^{-(2Y-2X-3)} \cdot K_o = \frac{C_{Cr^{VI}O_Y^{(2Y-6)-}} \cdot {C_{Q^4}}^{(2Y-2X-3)}}{C_{Cr^{III}O_x^{(3-2X)+}} \cdot {C_{O_2}}^{3/4} \cdot {C_{Q^3}}^{(2Y-2X-3)}} \qquad \text{B. 9}$$

Application to K_3

$$K_3 = \frac{a_{Q^2}}{a_{Q^3} \cdot {a_{Na_2O}}^{1/2}} \qquad \text{B. 10}$$

The constant K_s' can be easily deduced by appling the same procedure to K_3.

$$K_3 = \frac{a_{Q^2} \cdot K_4 \cdot C_{Q^4}}{a_{Q^3} \cdot C_{Q^3}} \qquad \text{B. 11}$$

$$K_s' = K_3 \cdot {K_4}^{-1} = \frac{C_{Q^2} \cdot C_{Q^4}}{{C_{Q^3}}^2} \qquad \text{B. 12}$$

This procedure created a new equilibrium between Q^4, Q^3 and Q^2.

Appendix C

Equation 22

The electrochemical potential corresponds to the following expression.

$$\tilde{\mu}_i = \mu_i + z_i V \qquad \text{C. 1}$$

The term $z_i V$ corresponds to the electric part (z_i being the electric charge and V the electric potential of the medium) and μ_i corresponds to the chemical part of the electrochemical potential.

Thus, the chemical diffusion is defined by the Nernst-Einstein equation as follow:

$$\overrightarrow{J_i^{Chemical}} = -\frac{D_i}{RT} C_i \overrightarrow{\nabla \mu_i} \qquad \text{C. 2}$$

The chemical potential gradient is defined by the activity.

$$\overrightarrow{\nabla \mu_i} = \overrightarrow{\nabla \left(\mu_i^0 + RT\, Ln(a_i) \right)} \qquad \text{C. 3}$$

Which can be developed:

$$\overrightarrow{\nabla \mu_i} = \frac{RT}{a_i} \overrightarrow{\nabla a_i} \qquad \text{C. 4}$$

By assuming that the activity is equal to the atomic fraction (ideal approximation).

$$a_i = \frac{C_i}{C_{total}} \qquad \text{C. 5}$$

$$\overrightarrow{\nabla a_i} = \frac{C_{total} \cdot \overrightarrow{\nabla C_i} - C_i \cdot \overrightarrow{\nabla C_{total}}}{{C_{total}}^2} \qquad \text{C. 6}$$

Thus, the chemical potential gradient corresponds to the following expression (C. 4, C. 5 C. 6).

$$\overrightarrow{\nabla \mu_i} = RT \left(\frac{\overrightarrow{\nabla C_i}}{C_i} - \frac{\overrightarrow{\nabla C_{total}}}{C_{total}} \right) \qquad \text{C. 7}$$

C. 7 and C. 2 lead to the expression of the equation 22.

$$\overrightarrow{J_i^{Chemical}} = -D_i \left(\overrightarrow{\nabla C_i} - \frac{C_i}{C_{total}} \overrightarrow{\nabla C_{total}} \right) \qquad \text{C. 8}$$

Appendix D

Equation 32-34

$$Na_2O_{\ \lambda}SiO_{2\ 1-\lambda} + O_2 \rightarrow Na_2O_{\ \chi}SiO_{2\ \gamma}O_{2\ \zeta} \quad \text{D. 1}$$

$$\chi + \gamma + \zeta = 1 \quad \text{D. 2}$$

The following ratio remains constant:

$$\frac{\chi}{\gamma} = \frac{\lambda}{1-\lambda} \quad \text{D. 3}$$

The concentration of oxygen in the liquid is:

$$C_{O_2} = H_{O_2} P_{O_2} \quad \text{D. 4}$$

The molar volume of the liquid is:

$$V_{m_{liquid}} = \chi V_{m_{Na_2O}} + \gamma V_{m_{SiO_2}} + \zeta V_{m_{O_2}} \quad \text{D. 5}$$

The concentration of oxygen can also be written as:

$$C_{O_2} = \frac{\zeta}{\chi V_{m_{Na_2O}} + \gamma V_{m_{SiO_2}} + \zeta V_{m_{O_2}}} \quad \text{D. 6}$$

D. 3, D. 4 and D. 6 lead to:

$$\left(1 + V_{m_{O_2}} H_{O_2} P_{O_2}\right)\zeta = H_{O_2} P_{O_2}\left(\chi V_{m_{Na_2O}} + \gamma V_{m_{SiO_2}}\right) \quad \text{D. 7}$$

And finally, D. 2, D. 3 and D. 7 lead to:

$$\zeta = \frac{H_{O_2} P_{O_2}\left(\frac{\lambda}{1-\lambda} V_{m_{Na_2O}} + V_{m_{SiO_2}}\right)}{1 + V_{m_{O_2}} H_{O_2} P_{O_2}} \gamma \quad \text{D. 8}$$

$$\chi = \frac{\lambda}{1-\lambda}\gamma \quad \text{D. 9}$$

$$\gamma = \left(\frac{1}{1-\lambda} + \frac{H_{O_2} P_{O_2}\left(\frac{\lambda}{1-\lambda} V_{m_{Na_2O}} + V_{m_{SiO_2}}\right)}{1 + V_{m_{O_2}} H_{O_2} P_{O_2}}\right)^{-1} \quad \text{D. 10}$$

The equations D. 8, D. 9 and D. 10 correspond to the equations eq. 32, eq. 33 and eq. 34 respectively.

Appendix E

Equation 37

$$\frac{C_{Cr^{III}}}{C_{Cr}^{App}} = P \qquad \text{E. 1}$$

The total amount of chromium corresponds to:

$$C_{Cr}^{App} = C_{Cr^{III}} + C_{Cr^{VI}} \qquad \text{E. 2}$$

Thus, the total flux of chromium is:

$$J_{Cr}^{App} = -D_{Cr^{III}} \frac{dC_{Cr^{III}}}{dx} - D_{Cr^{VI}} \frac{dC_{Cr^{VI}}}{dx} \qquad \text{E. 3}$$

Thanks to the equation E. 1 and E. 2, the equation E. 3 can be written as:

$$J_{Cr}^{App} = -D_{Cr^{III}} \frac{d(P)\, C_{Cr}^{App}}{dx} - D_{Cr^{VI}} \frac{d(1-P)\, C_{Cr}^{App}}{dx} \qquad \text{E. 4}$$

$$J_{Cr}^{App} = -D_{Cr}^{App} \frac{dC_{Cr}^{App}}{dx} \qquad \text{E. 5}$$

$$-D_{Cr}^{App} \frac{dC_{Cr}^{App}}{dx} = -\left(P \frac{dC_{Cr}^{App}}{dx} + C_{Cr}^{App} \frac{dP}{dx}\right) D_{Cr^{III}} - \left((1-P) \frac{dC_{Cr}^{App}}{dx} - C_{Cr}^{App} \frac{dP}{dx}\right) D_{Cr^{VI}} \qquad \text{E. 6}$$

$$-D_{Cr}^{App} \frac{dC_{Cr}^{App}}{dx} = -\left[\left(P + \frac{dP}{dC_{Cr}^{App}} C_{Cr}^{App}\right) D_{Cr^{III}} + \left(1 - P - \frac{dP}{dC_{Cr}^{App}} C_{Cr}^{App}\right) D_{Cr^{VI}}\right] \frac{dC_{Cr}^{App}}{dx} \qquad \text{E. 7}$$

The apparent diffusion coefficient can thus be easily identified:

$$D_{Cr}^{App} = \left(P + \frac{dP}{dC_{Cr}^{App}} C_{Cr}^{App}\right) D_{Cr^{III}} + \left(1 - P - \frac{dP}{dC_{Cr}^{App}} C_{Cr}^{App}\right) D_{Cr^{VI}} \qquad \text{E. 8}$$

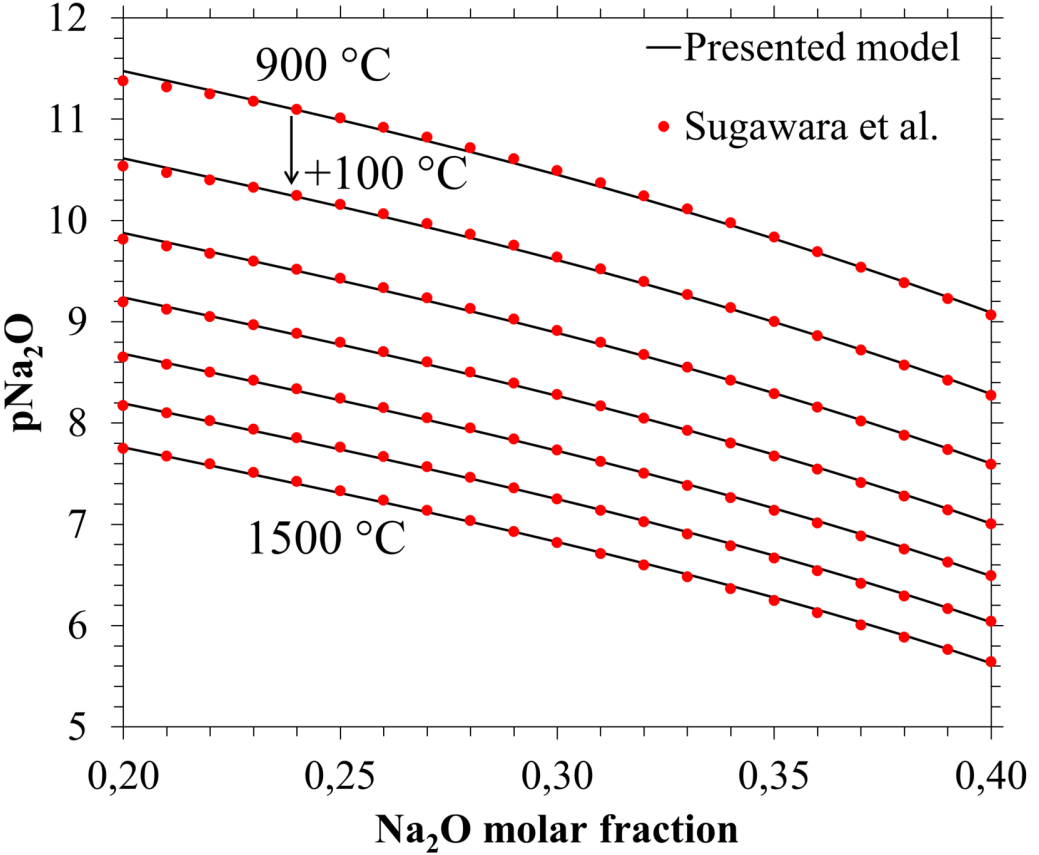
12
11
10
9
8
7
6
5
pNa2O
0,20
0,25
0,30
0,35
0,40
Na2O molar fraction
900 °C
+100 °C
1500 °C
Presented model
Sugawara et al.

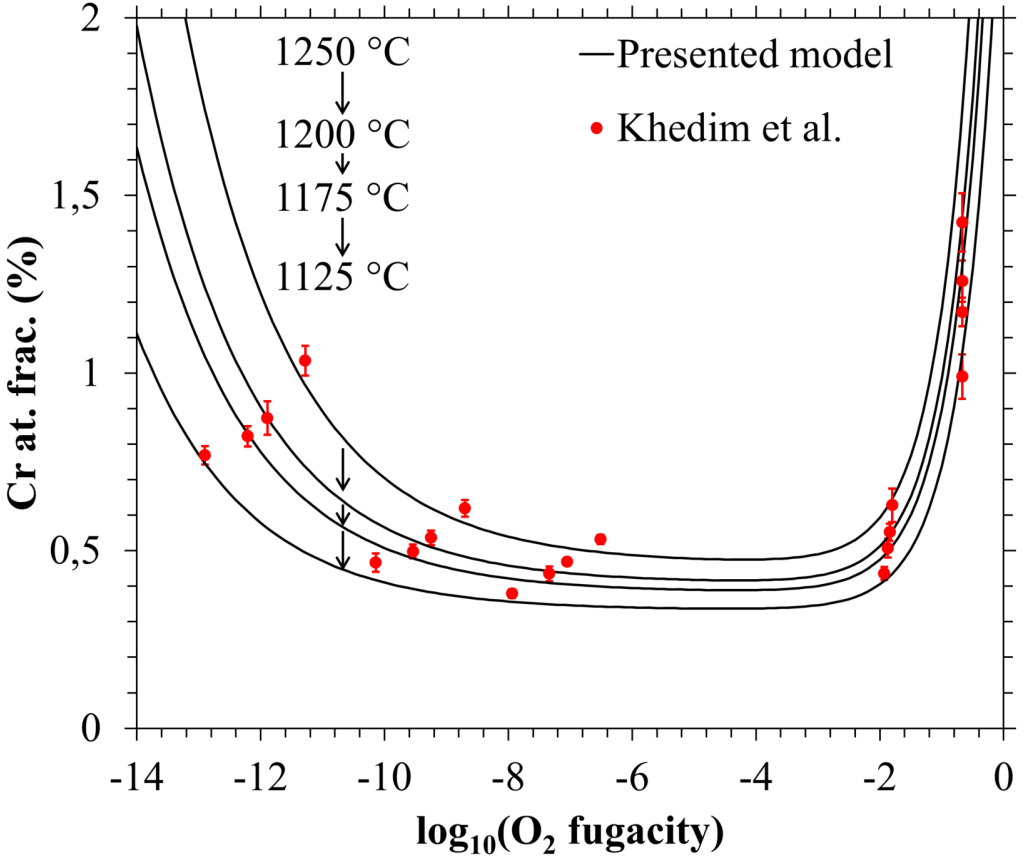
1250 °C
1200 °C
1175 °C
1125 °C
Presented model
Khedim et al.
Cr at. frac. (%)
log10(O2 fugacity)
2
1,5
1
0,5
0
-14
-12
-10
-8
-6
-4
-2
0

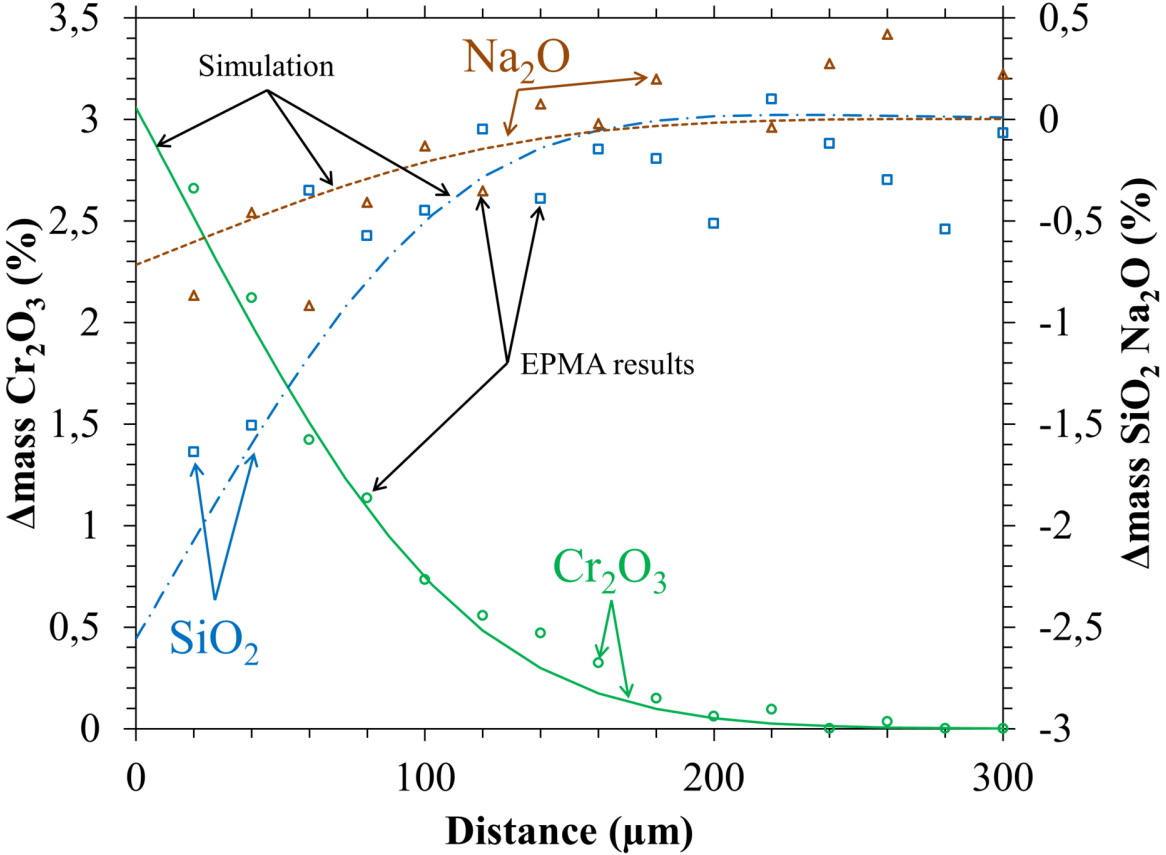
Simulation
Na_2O
EPMA results
Cr_2O_3
SiO_2
Δmass Cr_2O_3 (%)
Δmass SiO_2 Na_2O (%)
Distance (µm)
3,5
3
2,5
2
1,5
1
0,5
0
0,5
0
-0,5
-1
-1,5
-2
-2,5
-3
0
100
200
300

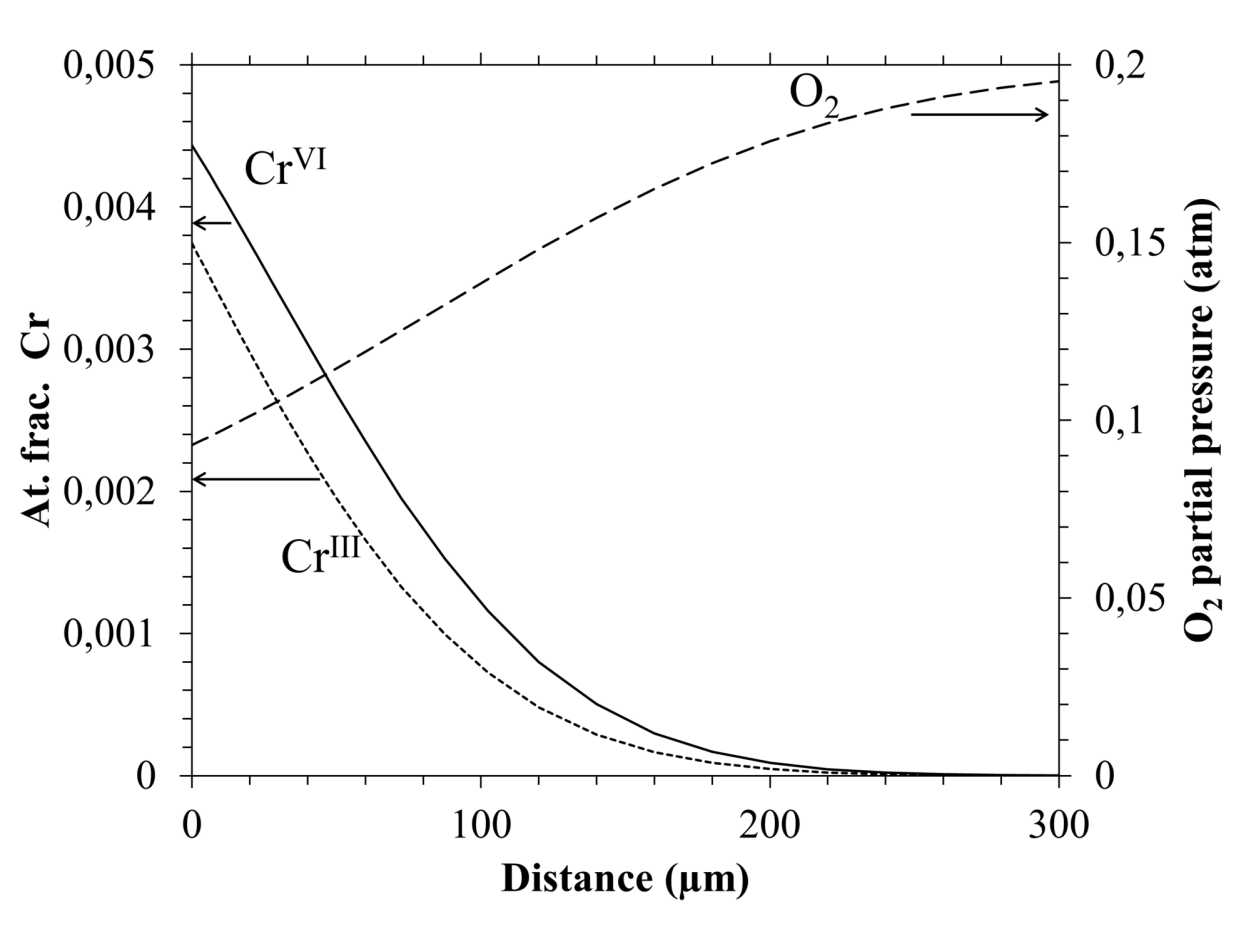
0,005
0,004
0,003
0,002
0,001
0
At. frac. Cr
0,2
0,15
0,1
0,05
0
O2 partial pressure (atm)
O2
Cr^VI
Cr^III
0
100
200
300
Distance (µm)

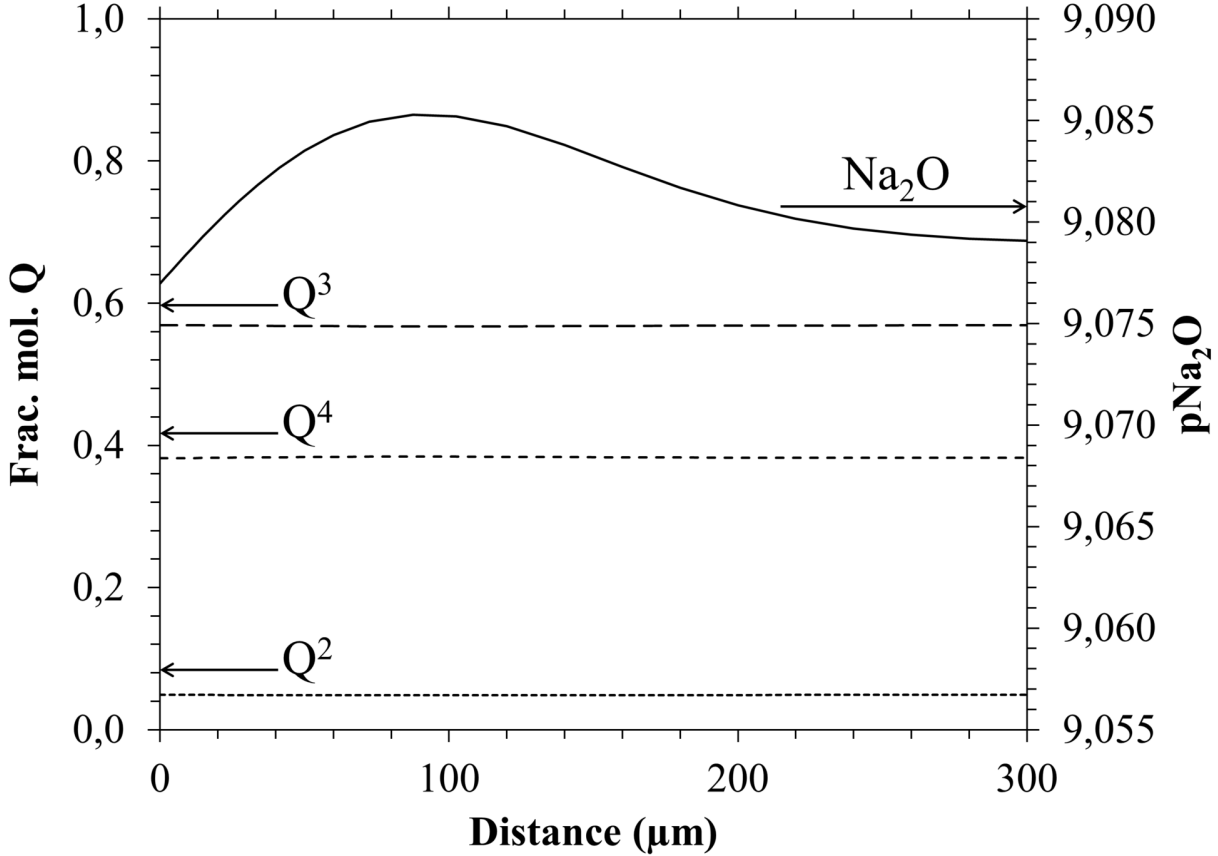
1,0
0,8
0,6
0,4
0,2
0,0
Frac. mol. Q
9,090
9,085
9,080
9,075
9,070
9,065
9,060
9,055
pNa2O
Na2O
Q3
Q4
Q2
0
100
200
300
Distance (µm)

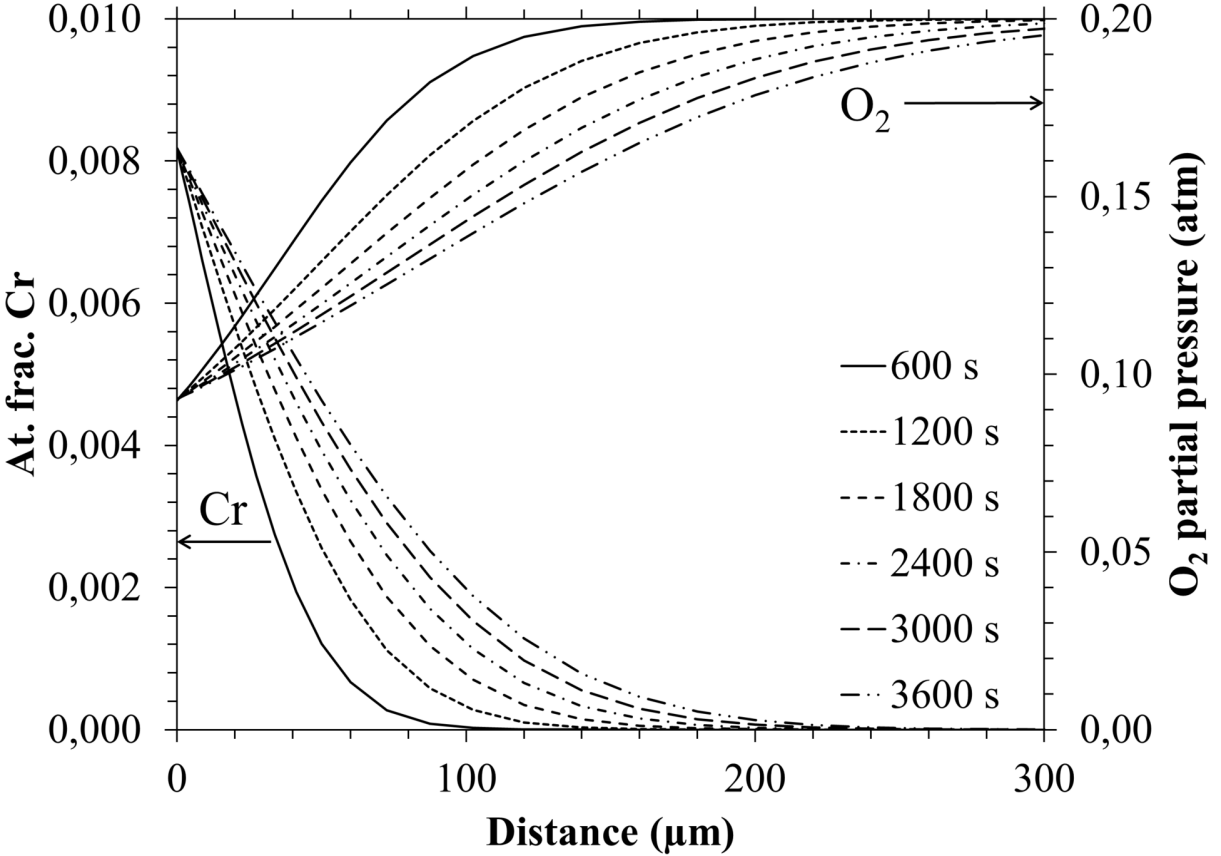
0,010
0,008
0,006
0,004
0,002
0,000
At. frac. Cr
0,20
0,15
0,10
0,05
0,00
O2 partial pressure (atm)
0
100
200
300
Distance (µm)
O2
Cr
600 s
1200 s
1800 s
2400 s
3000 s
3600 s

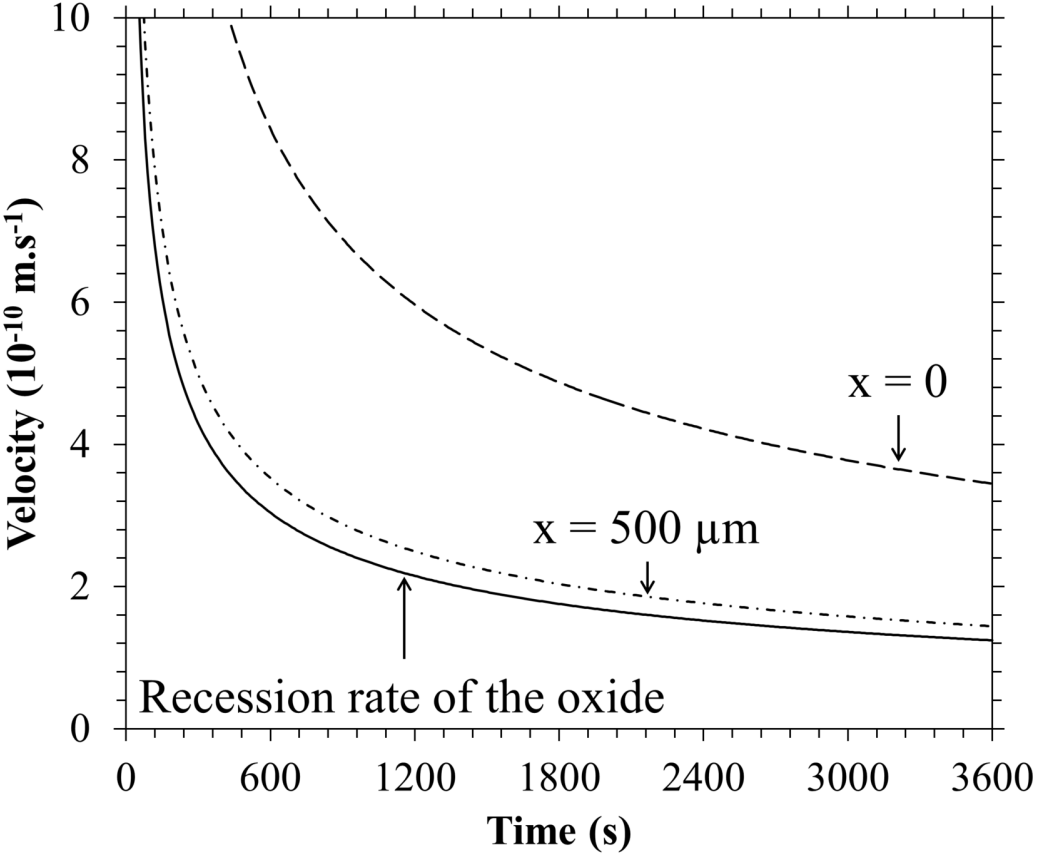
10
8
6
4
2
0
Velocity (10-10 m.s-1)
x = 0
x = 500 µm
Recession rate of the oxide
0
600
1200
1800
2400
3000
3600
Time (s)

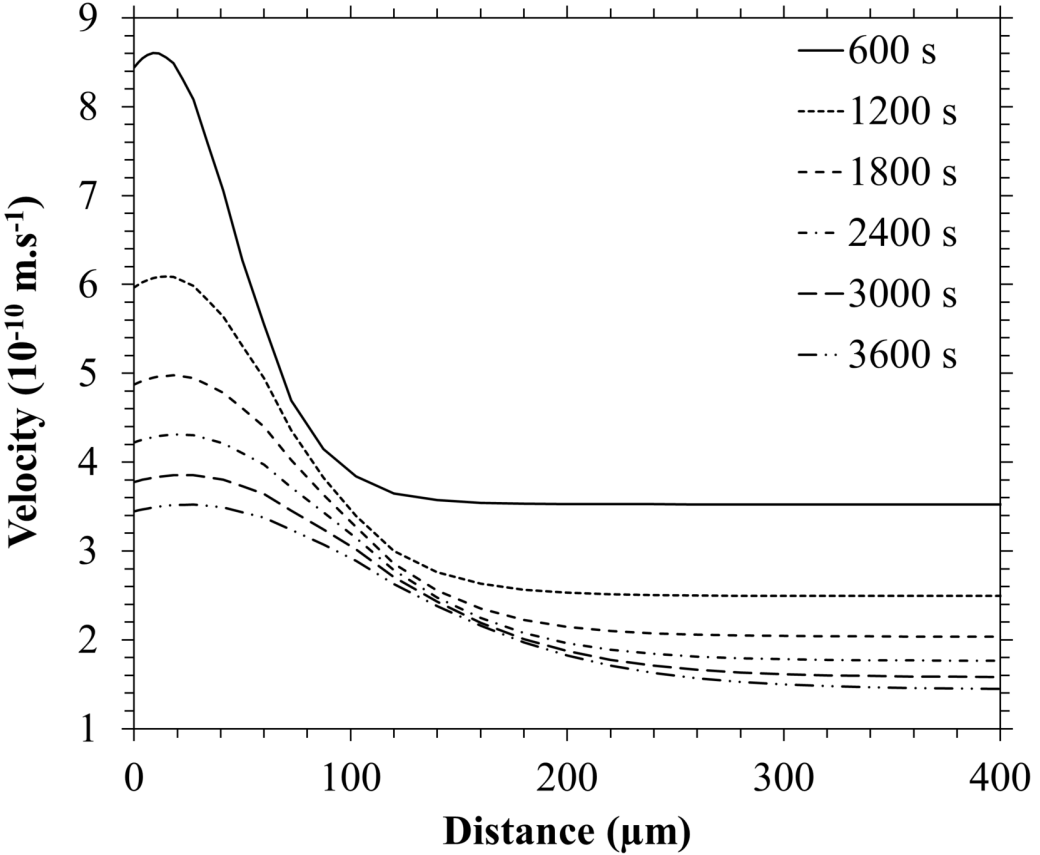
600 s
1200 s
1800 s
2400 s
3000 s
3600 s
Velocity (10-10 m.s-1)
Distance (µm)
9
8
7
6
5
4
3
2
1
0
100
200
300
400

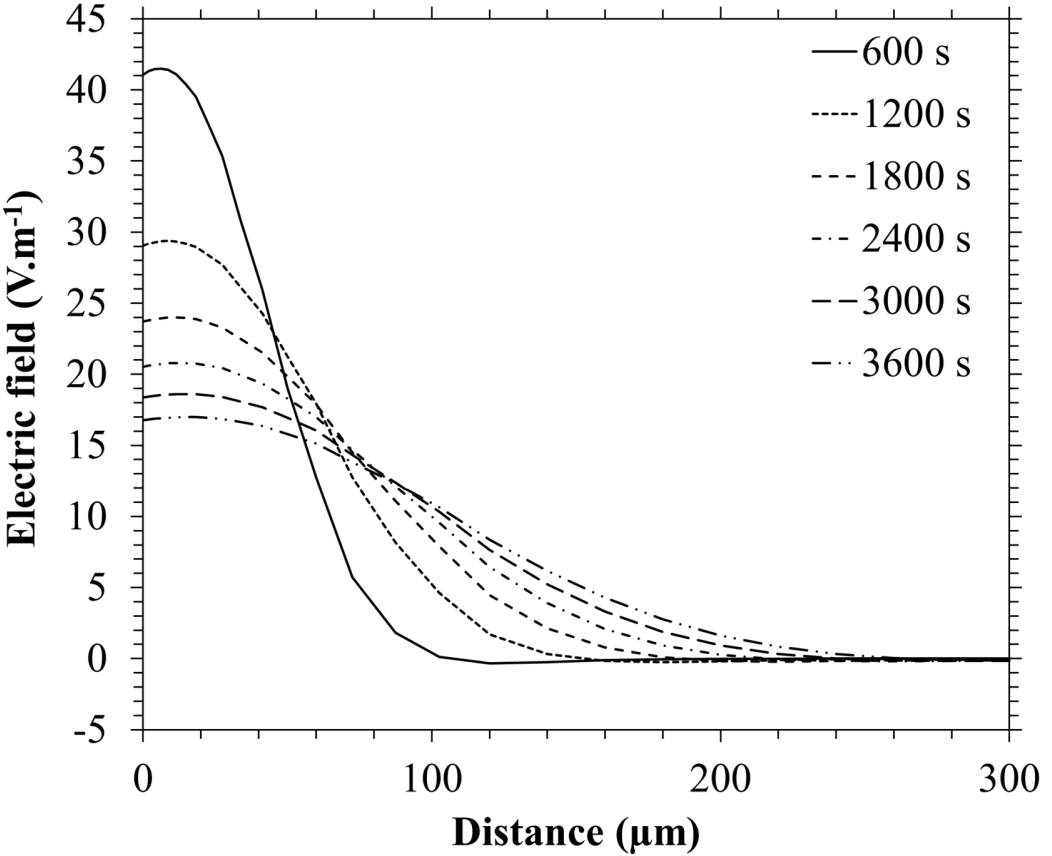
45
40
35
30
25
20
15
10
5
0
-5
0
100
200
300
Electric field (V.m-1)
Distance (µm)
600 s
1200 s
1800 s
2400 s
3000 s
3600 s

Tables

Table 1. Thermodynamic data determined in this study.

Reactions	ΔH (kJ.mol^{-1})	ΔS (J.mol^{-1}.K^{-1})	
$Q^4 + \frac{1}{2}Na_2O \overset{K_4}{\Leftrightarrow} Q^3$	-124.68	2.59	
$Q^3 + \frac{1}{2}Na_2O \overset{K_3}{\Leftrightarrow} Q^2$	-112.45	-12.52	
$\frac{1}{2}Cr_2O_{3\,cristal} \overset{K_d}{\Leftrightarrow} Cr^{III}O_X^{(3-2X)+} + \left(\frac{3}{2} - X\right)O^{2-}$	80.72	-14.06	X = 1.36
$Cr^{III}O_X^{(3-2X)+} + \frac{3}{4}O_2 + \left(Y - X - \frac{3}{2}\right)O^{2-} \overset{K_o}{\Leftrightarrow} Cr^{VI}O_Y^{(2Y-6)-}$	-54.46	40.50	Y = 3.22
$Cr^{III}O_X^{(3-2X)+} \overset{K_r}{\Leftrightarrow} Cr^{II}O_Z^{(2-2Z)+} + \frac{1}{4}O_2 + \left(X - Z - \frac{1}{2}\right)O^{2-}$	165.95	20.19	Z = 0.64

Table 2. Set of parameters used in the simulation.

Chemical species	D_i (m².s^{-1})	z_i (C/mol)	V_{m_i} (m^3.mol^{-1})
$Cr^{III}O_X^{(3-2X)+}$	1.3 10^{-12}	27020	2.91 10^{-5}
$Cr^{VI}O_Y^{(2Y-6)-}$	0.7 10^{-12}	-42460	3.70 10^{-5}
Cr_2O_3	0	0	2.91 10^{-5}
O_2	2.7 10^{-12}		2.46 10^{-5}
Q^4	1.0 10^{-12}		2.72 10^{-5}
Q^3		-96500	
Q^2		-193000	
Na^+	1.0 10^{-10}	96500	1.36 10^{-5}
Reaction rates			
kc_d	5 10^1		
kc_o	5 10^{-1}		
kc_s	1 10^{-2}		